Rheology of CO_2 – CH_4 hydrates measured in a concentric pressure cell

Jarand Gauteplass[1], Anja Torsvik[2], and Tanja Barth[1]

[1] University of Bergen, Department of Chemistry, Bergen, Norway
[2] SINTEF Petroleum, Department of Drilling and Well, Bergen, Norway

ABSTRACT

Gas hydrate formation may lead to increased flow resistance and complete plugging near CO_2 injection wells. To better understand this injectivity issue, we investigate gas flow properties in the hydrate stability zone. By using a rheological setup we have successfully formed, dissociated, and characterized hydrate slurries at realistic downhole conditions.

INTRODUCTION

Injection and storage of CO_2 in the subsurface is a highly relevant method of reducing the climate gas emissions into the earth's atmosphere. Depleted hydrocarbon reservoirs and saline aquifers are targeted as potential offshore storage sites. In this context, a high injectivity of CO_2 is critical in order to take advantage of the full storage capacity of the reservoir. Reported mechanisms causing loss in field injectivity near gas injection wells include hydrate formation[1] and salt precipitation[2]. Gas hydrates are clathrates, where water molecules encapsulate smaller guest molecules, e.g. CO_2 or CH_4, in an open structural lattice. If all the cages in the structure are filled, hydrate is composed of approximately 85 mol% water and 15 mol% gas[3]. Hydrates form at high pressures and low temperatures, and nucleation may result in increased flow resistance and plugging in pores. Typically, re-injected CO_2 contains a fraction of CH_4[4], causing the temperature range inside the hydrate stability zone (HSZ) to increase.

Earlier rheological studies on gas hydrates have mainly focused on hydrocarbon/water mixtures related to blockage of pipelines[5-9], and CO_2 hydrate slurry in refrigeration systems[10,11]. Rheological properties of gas hydrates associated with CO_2 injection and storage in the subsurface are uncharted territories. This paper focuses on CO_2/CH_4/water flow properties in the HSZ. We form, dissociate, and characterize gas hydrates directly in a modular compact rheometer fitted with a profiled bob, and a pressure cell with thermal regulations.

MATERIALS AND METHODS

Laboratory setup

The setup consists of an Anton Paar MCR102 rheometer, C-ETD 200/XL electrical temperature device, XL pressure cell, Keller PA-23SY 200 bar pressure transducer, Pt100 temperature log, PC w/ RheoPlus software, Julabo F32-ME refrigerated circulator, Teledyne Isco 65D syringe pumps, CPS VP6D vacuum pump, Leutert mixing cylinder, Leutert gas accumulator, and compressed CO_2 and CH_4 gas sources.

The rheometer pressure cell is completely sealed, and consists of a pressure cup, a pressure head, and a magnetic coupling. Maximum pressure and temperature in the pressure cell are respectively 150 bar and 180 °C. A refrigerated circulator supplies the rheometer with cooling fluid. The magnetic coupling transfers the torque from the rheometer drive to the pressure head where a

magnet is mounted on an axis. A grooved, flat-bottom bob (CC33.2-0-62/PR/P6-SN88732) designed for hydrate measurements is attached to the axis. This specific bob results in a sample volume of 14 ml in the pressure cell. The mechanical ball bearing system consists of an upper and a lower high-precision bearing. Torque deviations caused by the mechanical bearings are reduced to a minimum by averaging measurements over exactly one revolution[12].

Prior to hydrate measurements, the rheometer runs at constant shear rate for 1 hour to warm up the mechanical bearings, followed by an air check. The pressure cell is empty (evacuated) at this point. A motor adjustment and a precision air check with sine wave of ± 150 μNm conclude the pre-measurements.

Sample preparation

Deionized water and gas (CH_4 or CO_2) are prepared and pressurized separately before combining in a motorized mixing cylinder. The volumetric fraction in the cylinder is S_{water}= 0.6 and S_{gas}= 0.4. The mixing cylinder induces turbulent movement within the sample to accelerate the saturation process. Saturated water and gas are transferred to the rheometer, and displace the initial gas phase occupying the pressurized cell. The filling sequence and the transient period end when viscosity measurements reach a plateau, indicating a uniformly filled pressure cup.

Hydrate measurements

Hydrate formation: The pressurized and saturated fluids are cooled at a rate of 0.5 °C/min in the rheometer cell. The temperature decreases from 25 °C to set temperature of 2 °C in the closed system. Throughout the experiment, the rheometer runs at constant shear rate of 1200 s^{-1}. Software parameters are averaged over one revolution, and the measuring point duration is 20 seconds. Viscosity profiles and pressure logs determine the onset of hydrate nucleation and further growth.

Hydrate characterization: In the HSZ, a flow curve is established for a range of shear rates, typically from 700 – 1200 s^{-1}. Starting at the lowest shear rate, the system is ramped up to highest shear rate, held there for 10 measuring points, before being ramped down to initial conditions. Shear rate sweeps account for any history dependency of the hydrate slurry. Yield stress is measured after a simulated shut-in period of 1 hour. There are no pressure gradient or shear rate present during the shut-in. Measured yield stress on solidified hydrate occurs at controlled shear rate (CSR) operation from 10 to 1500 s^{-1}. The transition area is defined as the range where the relationship between strain and shear stress is no longer linear.

Hydrate dissociation: Hydrate dissociation in the pressure cell occurs by thermal stimulation. The heating rate is set to 0.5 °C/min and the closed system runs at constant shear rate of 1200 s^{-1}. Viscosity profiles and pressure logs determine the onset of hydrate dissociation.

Results presented in this paper are examples from a series of initial experiments. Several experiments in the HSZ did not lead to hydrate formation within a reasonable time scale (>20 hrs), and serve as hydrate-free baseline measurements. The repeatability of the experiments has not yet been properly determined.

RESULTS AND DISCUSSION

Gas hydrate stability depends on pressure, temperature, and composition. Hydrate equilibrium curves for three different gas compositions are simulated in Fig. 1. Typically, hydrates are thermodynamically stable at high pressures and low temperatures. The whole line represents a CH_4/water system, the dotted line a CO_2/water system, and the broken line a gas mixture of 95 mol% CO_2, 5 mol% CH_4/water system. The HSZ increases when adding small fractions of CH_4 in the CO_2 phase, compared to pure CO_2. This is highly

relevant because most re-injected CO_2 at the Norwegian Continental Shelf contains impurities, including CH_4. Adding thermodynamic inhibitors (e.g. salt or methanol) results in a shift of the equilibrium curve to the left. The experimental conditions are marked in Fig. 1, and are 60 bar (CO_2) and 75 bar (CH_4), at temperature of 2 °C, well within the HSZ for all gas compositions.

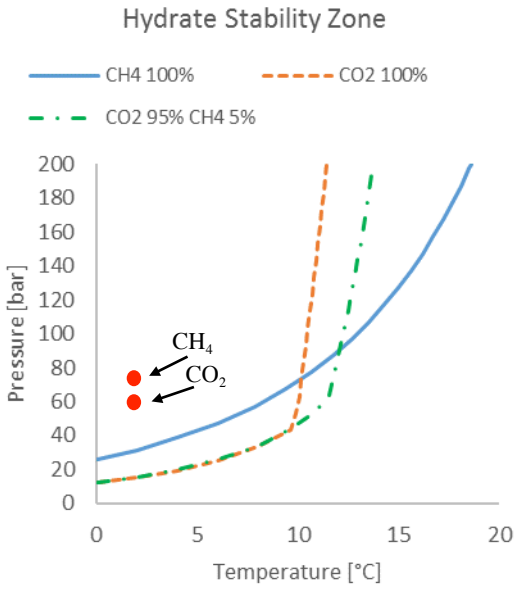

Figure 1. Hydrate (S_w=0.6) phase envelope for pure CH_4 (whole line), pure CO_2 (dotted line), and a blend of 95 mol% CO_2 and 5 mol% CH_4 (broken line), from PVTsim Nova 2 (SRK-Peneloux).

Hydrate cycle

Gas hydrates are formed and dissociated directly in the rheometer at constant volume. Measured parameters include shear rate, shear stress, torque, normal force, viscosity, pressure, and temperature. Fig. 2 maps a full cycle of hydrate formation and dissociation. The sample cools at a rate of 0.5 °C/min from starting point A to B. At point B the sample has reached the set temperature of 2 °C and the cell pressure has decreased following the temperature reduction. The induction time, defined as the time from the system has reached hydrate stable conditions until hydrate nucleation occurs, is in this case approximately 2.2 hours. During hydrate formation (point B to C), the system pressure is reduced as gas molecules contained in hydrates have a much higher density than free gas molecules.

Hydrate formation is an exothermic process, however, the heat released here is barely measurable (a small deviation toward right can be seen on the graph) because the Peltier jacket maintains a constant temperature in the cell. The viscosity measurements combined with pressure readings define the onset of hydrate nucleation (Fig. 3), hydrate redistribution (Fig. 4), and hydrate dissociation (Fig. 7).

At point C, we characterize hydrate rheology by measuring steady-state flow curves (Fig. 5) and yield stress (Fig. 6). From point C, the temperature increases by 0.5 °C/min and the sudden pressure increase at point D indicates the onset of hydrate dissociation. Further dissociation takes place on the line from point D to E, following the same path as the hydrate equilibrium curve (CH_4, whole line) in Fig. 1. The reason for the offset between measured and simulated dissociation temperatures is likely due to a "kinetic" effect in the metastable zone. There is a temperature lag in the experimental system at the given heating rate, because the temperature is measured in the wall of the pressure cell rather than in the annulus[12].

Point E represents the end of hydrate dissociation. The temperature continues to increase at constant heating rate from point E to the final point, F, causing the pressure to nearly return to the initial state prior to hydrate formation.

Hydrate formation

Hydrate formation is a stochastic process, and the induction time varies with key parameters such as subcooling, fluid composition, contact area/interfaces, capillary pressure, and surface roughness. Fig. 3 illustrates the varying induction times.

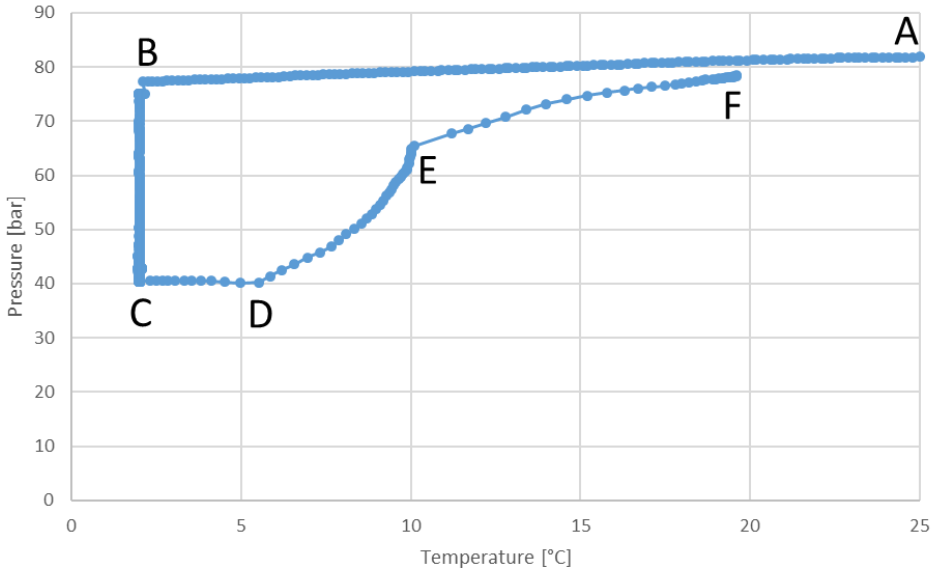

Figure 2. P-T mapping of a CH_4 hydrate cycle (S_w=0.6) at constant shear rate (1200 s^{-1}). The path A to B represent a cooling period, B to C hydrate formation, C to F thermal stimulation, and D to E hydrate dissociation.

Here, significant viscosity build-ups ascribed to hydrate formation in three experiments (Exp. 1; CH_4 at 75 bar, Exp. 2; CH_4 at 75 bar, and Exp. 3; CO_2 at 60 bar) are captured in the early stage of the cycle (< 3 hrs). Induction time is approximately 0.8, 0.9, and 2.2 hours for respectively Exp. 2, 3, and 1. Growth of hydrate crystals occurred at 2 °C.

In Exp. 1, an initial shear rate of 600 s^{-1} was selected. As this resulted in no hydrate formation within the HSZ after 20 hours, we increased the shear rate to 1200 s^{-1} to facilitate enhanced motion/dispersion. Hydrates formed after 2.2 hours, and 1200 s^{-1} became the default shear rate in the following experiments.

The slope of the viscosity profiles are different for all three experiments. CO_2 hydrates responded in the steepest profile, indicating rapid hydrate formation. Crystal growth of hydrate accelerates with increasing distance from the equilibrium curve and into the HSZ (degree of subcooling). Exp. 1 and 2 (CH_4 hydrate) were conducted at identical pressure and temperature, however, they developed quite different in terms of flow resistance. The long induction time associated with Exp. 1 is likely influenced by the previously mentioned change of shear rate.

Both CO_2 and CH_4 guest molecules form structure I (sI) hydrates, consisting of 6 large and 2 small cavities in each unit cell. CH_4 molecules have the possibility to fill all 8 cavities, whereas the larger CO_2 molecules typically fill only 6 cavities. This difference in hydrate composition (CO_2 sI will have a higher water fraction than CH_4 sI hydrate) may influence the flow resistance measured. Hydrate slurry viscosity has been reported to increase with an increasing water content[8]. More importantly, there is an uncertainty in material balance during sample transport from the mixing cylinder to the rheometer due to gravity segregation. Therefore, the final water content in the pressure cell may not reflect precisely the initial water content in the mixing cylinder.

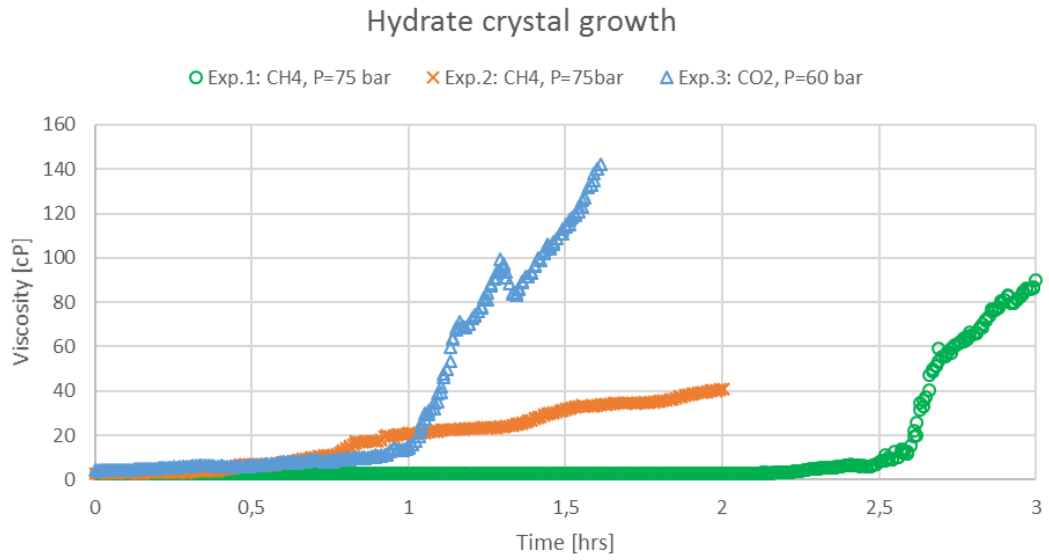

Figure 3. Hydrate nucleation and early growth for CH_4 hydrate (Exp. 1 and 2) and CO_2 hydrate (Exp. 3) at water fraction S_w=0.6 and temperature 2 °C. Induction time is approximately 0.8 hours (Exp. 2), 0.9 hours (Exp. 3), and 2.2 hours (Exp. 1).

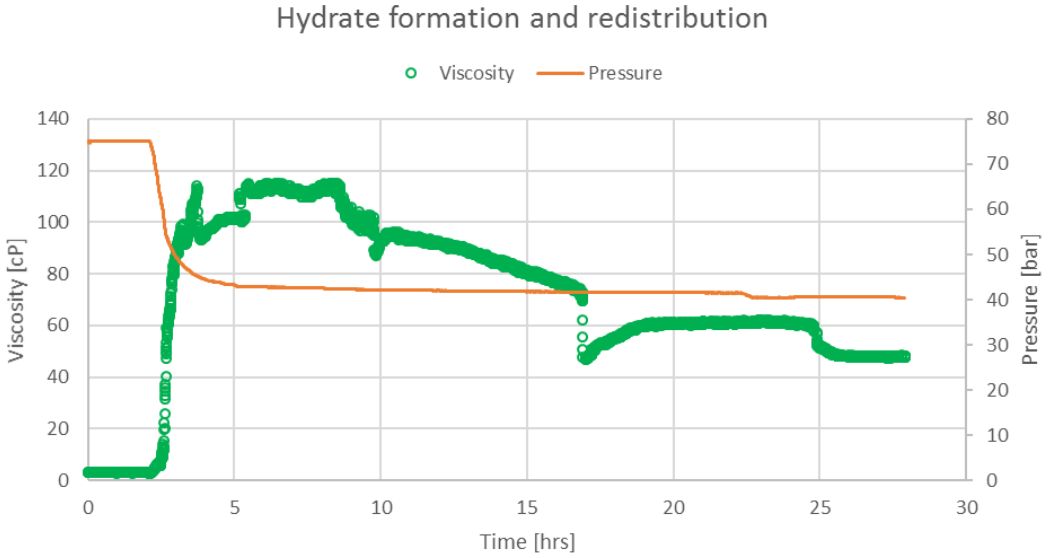

Figure 4. CH_4 hydrate (S_w=0.6) formation and redistribution (Exp. 1) at constant temperature (2 °C) and shear rate (1200 s^{-1}). Viscosity (circle) and pressure (line) define nucleation, growth, and redistribution of hydrate slurry in the concentric pressure cell.

A full viscosity profile capturing the formation and maturation of CH_4 hydrate (Exp. 1) is shown in Fig. 4. The pressure and viscosity are stable for the first 2.2 hours in the HSZ. Hydrate slurry viscosity increased rapidly after the induction period (by a factor of ~ 40), followed by a decay in viscosity ascribed to hydrate redistribution and hydrate maturation. The suspension peaks sharply in viscosity around 3.7 hours in Fig. 4. The subsequent erratic viscosity behavior is possibly due to jam and slip of hydrate

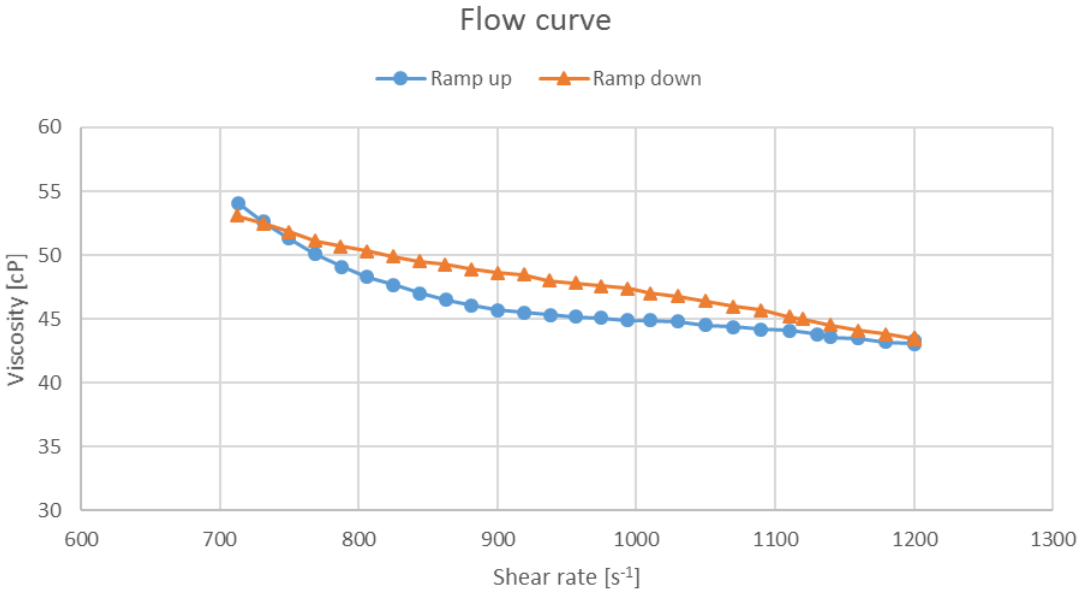

Figure 5. Flow curve for CH_4 hydrate at 2 °C and 40 bar (point C in Figure 2). The hydrate slurry (S_w=0.6) demonstrates a shear-thinning behavior and a hysteresis area is present in the shear rate sweep from 700 s^{-1} to 1200 s^{-1} (circle) and from 1200 s^{-1} to 700 s^{-1} (triangle).

aggregates, as their size approaches the width of the annulus[8]. Because the system is closed, the pressure directly reflects hydrate formation (pressure decrease) and hydrate dissociation (pressure increase) in the couette cylinder. The pressure stabilizes around 5 hours, after this no significant hydrate formation occurs. This means that the following viscosity variations are due to breakup or rearrangement of hydrate aggregates.

Mature hydrates have a lower flow resistance than newly formed hydrates. After 24 hours, the viscosity is around 50% of the initial viscosity peak. A shift in hydrate structure on the pore-level has been reported within a similar time frame[13], which may influence the suspension viscosity. A possible explanation is the presence of initially wet ("sticky") hydrate particles that slowly dries as hydrate matures[6]. More specifically, water is trapped and immobilized during agglomeration, causing the effective volume to increase. When breaking up, the interstitial water is mobilized, decreasing the effective aggregate volume, and thus decreasing the viscosity[14]. Hydrate aggregates continually break up and coalesce in the shear field.

Hydrate characterization

Gas hydrates were characterized in the HSZ at constant temperature and pressure. An example of a flow curve is given in Fig. 5. Hydrate viscosity was measured in series starting at 700 s^{-1} to 1200 s^{-1}, held at 1200 s^{-1}, and from 1200 s^{-1} to 700 s^{-1}. Both ramp up and ramp down tests demonstrate that the viscosity decreases with an increasing shear rate, i.e. the slurry is shear-thinning. A hysteresis effect is present in the flow curve, the ramp down path deviates from the ramp up path. This hysteresis area in Fig. 5 indicates that the slurry exhibits a time-dependent behavior. The result is consistent with other rheological studies on gas hydrates[5,6,7,8].

In shut-in and restart situations, hydrates are allowed to anneal and can cause significant problems in terms of blockages. Hydrate flowability may be estimated by yield stress in such situations[8]. Yield stress

was measured on solidified hydrate after a 1-hour shut-in period, shown in Fig. 6. Here, strain and shear stress are mapped at controlled shear rate (CSR) from 10 to 1500 s^{-1}. The yield point of the hydrate is where the strain-stress curve deflects from linearity, representing the transition area between elastic stretching and flow. The hydrate yields at approximately 300 Pa in Fig. 6. The significant yield pressure generated after only 1 hour implies a high risk of hydrate plugging under operational stoppage.

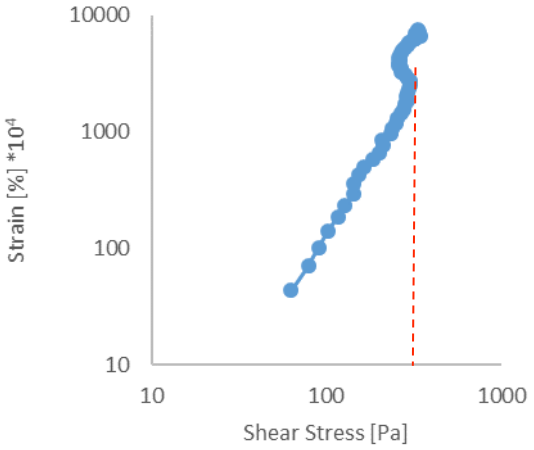

Figure 6. The CO_2 hydrate yield point is approximately 300 Pa after 1 hour.

Hydrate dissociation

Hydrate dissociation occurred by thermal stimulation at 0.5 °C/min heating rate and 1200 s^{-1} shear rate. Examples of hydrate dissociation profiles are presented in Fig. 7. CO_2 hydrate (triangle) and CH_4 hydrate (circle) are compared to a baseline CO_2/water (line) experiment where no hydrate formed. The onset of hydrate dissociation is at approximately 5.6 °C for CH_4 hydrate and 11.7 °C for CO_2 hydrate, within the metastable region for the equilibrium curves in Fig. 1.

Measured hydrate viscosity gradually decreases as temperature increases, until the dissociation temperature is reached, resulting in a well-defined drop in viscosity. A local viscosity peak is observed in the ongoing dissociation process at 8.4 °C for CH_4 hydrate and 12.6 °C for CO_2 hydrate. For CO_2 hydrate, the viscosity also increases just before the dissociation temperature. This is likely caused by increased "stickiness" associated with premelt of hydrate particles as reported by others[6,8]. The viscosity profiles of CO_2 hydrate and CH_4 hydrate coincide with the baseline experiment after the dissociation is completed.

CONCLUSIONS

We successfully formed and dissociated gas hydrates directly in a concentric cylinder. Viscosity profiles captured the significant nucleation, growth and agglomeration of the hydrates. Likely field scale implications are reduced gas injectivity in the hydrate stability zone. Hydrate slurry viscosity increased rapidly after the induction period, followed by a decay in viscosity ascribed to hydrate redistribution and hydrate maturation. Hydrates were consistently shear-thinning and demonstrated hysteresis effects from flow curves. Measured yield stress gave valuable insight in hydrate agglomeration during shutdowns. Hydrate dissociation occurred when the system was heated and corresponded with predictions using a thermodynamic modeling tool.

We find that the combination of a modular compact rheometer, a grooved bob, and a pressure cell with thermal regulations is well suited for characterization of gas hydrates.

ACKNOWLEDGMENTS

The experiments were designed and conducted at the SINTEF fluid laboratory in Bergen, and at the Department of Chemistry, University of Bergen. The authors are indebted to the Research Council of Norway for financial support under CLIMIT project number 255490.

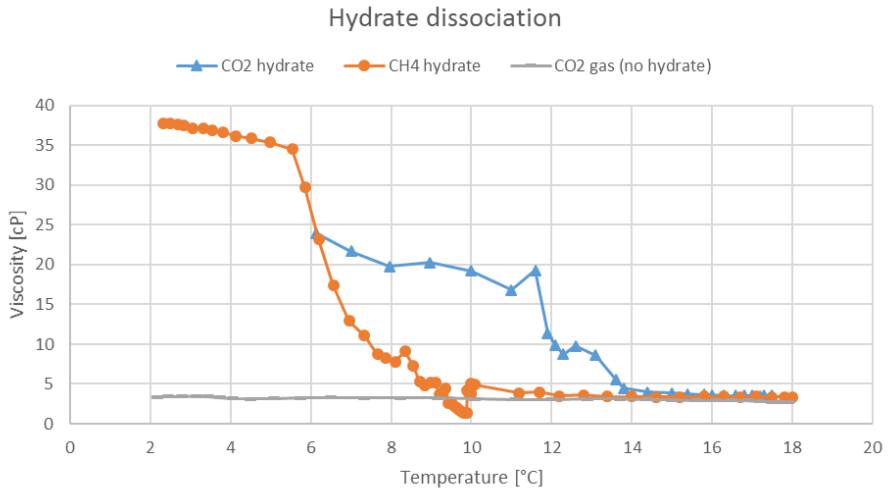

Figure 7. Hydrate dissociation for CO_2 hydrate (triangle, 60 bar), and CH_4 hydrate (circle, 40 bar), compared to baseline CO_2 gas (line, 40 bar).

REFERENCES

1. Awan AR, Teigland R, Kleppe J. (2008) "A Survey of North Sea Enhanced-Oil-Recovery Projects Initiated During the Years 1975 to 2005", SPE Res.Eng., **11**(3), 497-512.

2. Hansen O, Gilding D, Nazarian B, Osdal B, Ringrose P, Kristoffersen J-B, et al. (2013) "Snøhvit: The History of Injecting and Storing 1 Mt CO2 in the Fluvial Tubåen Fm", *Energy Procedia*., **37**, 3565-73.

3. Sloan ED (1998) "Gas Hydrates: Review of Physical/Chemical Properties", *Energy & Fuels*, **12**(2), 191-6.

4. Eiken O, Ringrose P, Hermanrud C, Nazarian B, Torp TA, Høier L. (2011) "Lessons learned from 14 years of CCS operations: Sleipner", In Salah and Snøhvit. *Energy Procedia*., **4**, 5541-8.

5. Sinquin A, Palermo T, Peysson Y. (2004) "Rheological and Flow Properties of Gas Hydrate Suspensions", *Oil & Gas Science and Technology*, **59**, 41-57.

6. Schuller R, Tande M, Kvandal H-K. (2005) Rheological hydrate detection and characterization. *ATNRS*, **13**, 83-90.

7. Hald K, Nuland S. (2007) "Hydrate slurry rheology in the petroleum industry", *ATNRS*., **15**.

8. Webb EB, Rensing PJ, Koh CA, Sloan ED, Sum AK, Liberatore MW. (2012) "High-Pressure Rheology of Hydrate Slurries Formed from Water-in-Oil Emulsions", *Energy & Fuels*, **26**(6), 3504-9.

9. Fidel-Dufour A, Gruy F, Herri J-M. (2006) "Rheology of methane hydrate slurries during their crystallization in a water in dodecane emulsion under flowing", *Chemical Engineering Science*, **61**(2), 505-15.

10. Jerbi S, Delahaye A, Oignet J, Fournaison L, Haberschill P. (2013) "Rheological properties of CO2 hydrate slurry produced in a stirred tank reactor and a secondary refrigeration loop", *Int.J. of Refrigeration*, **36**(4), 1294-301.

11. Delahaye A, Fournaison L, Marinhas S, Martínez MC. (2008) "Rheological study of hydrate slurry in a dynamic loop applied to secondary refrigeration", *Chemical Engineering Science*, **63**(13), 3551-9.

12. Heyer P, Arnold G, Wollny K. Anton Paar GmbH Application Report: "Guideline for the Pressure Cell".

13. Hauge LP, Gauteplass J, Høyland MD, Ersland G, Kovscek A, Fernø MA. (2016) "Pore-level hydrate formation mechanisms using realistic rock structures in high-pressure silicon micromodels", *Int. Journal of Greenhouse Gas Control*, **53**, 178-86.

14. Pal R. Rheology of simple and multiple emulsions. Current Opinion in Colloid & Interface Science. 2011;**16**(1):41-60.